IIETA International Information and Engineering Technology Association
Advancing the World of Information and Engineering

Journal Européen des Systèmes Automatisés
Vol. 59, No. 4, April, 2026, pp. 871-880
Journal homepage: http://iieta.org/journals/jesa

Mixed-Sensitivity H_∞ Voltage Regulation of a Boost DC–DC Converter with Integral Augmentation: Design and LQR Benchmarking

Belgacem Bekkar*, Khaled Ferkous, Abderrahmane Bellaouar

Laboratory of Materials, Energy Systems Technology and Environment Research Laboratory (MESTEL) University of Ghardaia, Ghardaia 47000, Algeria

Corresponding Author Email: bekkar.belgacem@univ-ghardaia.edu.dz

Copyright: ©2026 The authors. This article is published by IIETA and is licensed under the CC BY 4.0 license (http://creativecommons.org/licenses/by/4.0/).

https://doi.org/10.18280/jesa.590402

Received: 25 January 2026
Revised: 28 March 2026
Accepted: 10 April 2026
Available online: 30 April 2026

Keywords:
Boost converter, mixed-sensitivity H_∞ synthesis, integral augmentation, Linear Quadratic Regulator, robust voltage regulation

ABSTRACT

Boost DC-DC converters are widely used in renewable-energy and high step-up power-conditioning interfaces, but accurate voltage regulation remains challenging because of non-minimum-phase dynamics and strong operating-point dependence. This paper presents an integral-augmented mixed-sensitivity H_∞ controller for output-voltage regulation of a continuous-conduction-mode Boost converter subject to reference variations, load disturbances, and input-voltage perturbations. A control-oriented averaged small-signal model is first derived and augmented with an integral state to enforce zero steady-state tracking error. The controller is then synthesized within a mixed-sensitivity loop-shaping framework and benchmarked against a Linear Quadratic Regulator (LQR) controller designed from the same augmented nominal model. The final comparison is carried out in a nonlinear PWM switching model in order to assess regulation performance beyond the linear synthesis stage. The results show that the proposed controller provides faster and better damped reference tracking, reducing the worst-case rise time from 7.03 ms to 3.17 ms, the worst-case overshoot from 3.98% to 0.41%, and the worst-case settling time from 44.88 ms to 6.04 ms relative to the LQR benchmark. The largest improvement is obtained under abrupt load changes, where the output-voltage dip is reduced from 52.27 V to 32.16 V and the recovery time from 30.18 ms to 5.69 ms. Under a -10 V input-voltage disturbance, the proposed controller also decreases the voltage dip from 23.79 V to 8.24 V and shortens the recovery time from 13.62 ms to 2.63 ms. These simulation-based results indicate that integral-augmented mixed-sensitivity H_∞ synthesis provides a more favorable compromise among tracking speed, disturbance rejection, and admissible control effort for high-precision Boost-converter voltage regulation.

1. INTRODUCTION

The increasing penetration of photovoltaic (PV) generation and other DC-based energy systems, such as DC microgrids, battery energy storage interfaces, and grid-tied power-electronic converters, has intensified the demand for high-efficiency DC-DC conversion with fast and reliable voltage regulation [1, 2]. In such systems, the DC-DC stage acts as a dynamic actuator responsible for maintaining DC-bus voltage stability under load transients, source intermittency, and parameter variations. The Boost converter is widely used to interface low-voltage sources with higher-voltage DC buses; however, in continuous conduction mode (CCM), its duty-to-output dynamics include a right-half-plane (RHP) zero and exhibit pronounced operating-point dependence. These characteristics constrain the achievable bandwidth and complicate robust regulation [3, 4].

Industrial practice often relies on fixed-structure proportional-integral/proportional-integral-derivative (PI/PID) compensators and lead-lag designs because of their simplicity, but their performance may deteriorate when the operating point varies, leading to increased overshoot, longer settling times, and reduced robustness under line and load disturbances [5, 6]. In contrast, state-space averaging and small-signal linearization provide a control-oriented basis for systematic converter design [4, 7, 8]. Within this framework, optimal state-feedback methods such as Linear Quadratic Regulator (LQR) can improve nominal transient performance, whereas mixed-sensitivity H_∞ synthesis provides a more explicit frequency-domain framework for balancing tracking accuracy, disturbance attenuation, and control effort under non-minimum-phase constraints [9-13].

Recent literature confirms continuing interest in robust H_∞-based control for Boost and Boost-derived converter topologies, including high-gain Boost converters, interleaved Boost converters, and recent two-phase interleaved Boost applications in battery energy storage systems [14-17]. More broadly, recent robust H_∞ regulation results in related power-electronic applications also confirm the continuing relevance of frequency-domain robust design in converter control [18, 19]. These studies demonstrate the value of robust control for converter regulation; however, they do not always incorporate the tracking-error integral state directly into the synthesis model, and they rarely provide a transparent benchmark

against an optimal controller designed from the same augmented plant and assessed under matched operating scenarios. Consequently, the source of the observed performance differences often remains difficult to isolate.

The contribution of this paper is not the isolated use of mixed-sensitivity H_∞ control, integral augmentation, or LQR benchmarking, each of which is already established in the literature. Rather, the novelty lies in a controlled and methodologically consistent Boost-converter study that combines these elements within a common evaluation framework. First, the proposed controller is synthesized from an integral-augmented nominal small-signal model so that zero steady-state tracking error is enforced directly within the robust-design stage. Second, the LQR benchmark is constructed from the same augmented nominal plant, allowing differences in closed-loop behavior to be attributed to the control methodology rather than to differences in model structure. Third, the two controllers are assessed under identical reference, load, and input-voltage scenarios in a nonlinear PWM switching model using unified transient, disturbance, and actuator-related metrics. In this way, the paper aims to provide a fair and practically meaningful assessment of mixed-sensitivity H_∞ design for Boost-converter voltage regulation.

The remainder of this paper is organized as follows. Section II derives the averaged small-signal model and its integral augmentation. Section III presents the mixed-sensitivity H_∞ synthesis, the frequency-domain analysis, and the LQR benchmark. Section IV reports the comparative nonlinear simulation results, and Section V concludes the paper.

2. BOOST CONVERTER MODELING FOR CONTROL DESIGN

The electrical model of the Boost converter considered in this study is depicted in Figure 1. The circuit consists of an input voltage source V_g, an inductor L with series resistance r_L, an output capacitor C with equivalent series resistance r_C, a resistive load R_L, an ideal diode, and a controlled power switch. The inductor current is denoted by $i_L(t)$, the capacitor voltage by $v_C(t)$, the output voltage across the load network by $v_o(t)$, and the control input by $u(t)$, defined as the duty ratio of the pulse-width modulation (PWM) signal applied to the switch.

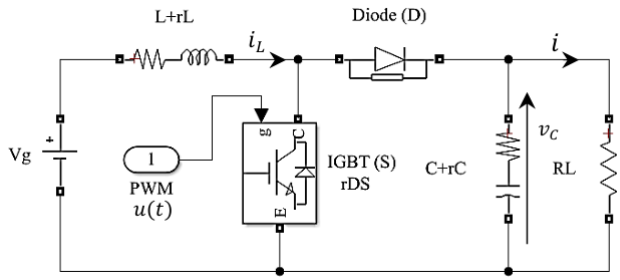

Figure 1. Electrical schematic of the Boost DC–DC converter

In the present work, an IGPT is adopted as the switching device. Alternative semiconductor devices may also be employed depending on voltage and current ratings, switching frequency, efficiency requirements, and cost constraints. For control-oriented modeling, the diode is assumed ideal, such that its forward voltage drop and reverse-recovery effects are neglected.

Under CCM, the boost converter is represented as a switched linear state-space system with two operating configurations associated with the switch position [4]:

$$\begin{cases} \dot{\mathrm{x}}(t) = \mathrm{A_i}\,\mathrm{x}(t) + \mathrm{B_i}\,V_g, \\ v_o(t) = \mathrm{C_i}\,\mathrm{x}(t), \end{cases} \qquad i \in \{1,2\}, \tag{1}$$

where, $\mathrm{x}(t) = [i_L(t) \quad v_C(t)]^{\mathrm{T}}$ is the state vector. The output voltage $v_o(t)$ denotes the voltage across the load network and therefore includes the effect of the capacitor ESR r_C.

$$\mathrm{A_1} = \begin{bmatrix} -\dfrac{r_L + r_{DS}}{L} & 0 \\ 0 & -\dfrac{1}{C(R_L + r_C)} \end{bmatrix}, \quad \mathrm{B_1} = \begin{bmatrix} \dfrac{1}{L} \\ 0 \end{bmatrix}, \quad \mathrm{C_1} = \begin{bmatrix} 0 & \dfrac{R_L}{R_L + r_C} \end{bmatrix}. \tag{2}$$

Switch OFF (open): The diode becomes forward-biased, transferring inductor energy to the output network. The corresponding matrices are:

$$\mathrm{A_2} = \begin{bmatrix} -\dfrac{R_L(r_L + r_C) + r_L r_C}{L(R_L + r_C)} & -\dfrac{R_L}{L(R_L + r_C)} \\ \dfrac{R_L}{C(R_L + r_C)} & -\dfrac{1}{C(R_L + r_C)} \end{bmatrix}, \quad \mathrm{B_2} = \begin{bmatrix} \dfrac{1}{L} \\ 0 \end{bmatrix}, \quad \mathrm{C_2} = \begin{bmatrix} \dfrac{R_L r_C}{R_L + r_C} & \dfrac{R_L}{R_L + r_C} \end{bmatrix}. \tag{3}$$

2.1 Averaged model

To obtain the continuous-time averaged model used for control synthesis, the switched dynamics in Eqs. (2)-(3) are averaged over one switching period using the duty ratio D and its complement $\bar{D} = 1 - D$:

$$\begin{aligned} \mathrm{A} &= \mathrm{A_1}D + \mathrm{A_2}\bar{D} \\ \mathrm{B} &= \mathrm{B_1}D + \mathrm{B_2}\bar{D} \\ \mathrm{C} &= \mathrm{C_1}D + \mathrm{C_2}\bar{D} \end{aligned} \tag{4}$$

The averaged model is linearized about a steady-state operating point under the assumption of small perturbations, yielding the small-signal representation of the Boost converter in [4]:

$$\begin{cases} \dot{\tilde{\mathrm{x}}}(t) = \mathrm{F}\,\tilde{\mathrm{x}}(t) + \mathrm{G}\,\tilde{d}(t), \\ \tilde{v}_o(t) = \mathrm{H}\,\tilde{\mathrm{x}}(t) + \mathrm{E}\,\tilde{d}(t) \end{cases} \tag{5}$$

where, $\tilde{\mathrm{x}}$ denotes the state perturbation, $\tilde{v}_o(t)$ is the output-voltage perturbation, and $\tilde{d}(t)$ is the duty-ratio perturbation about the nominal duty ratio D. The small-signal matrices are given by:

$$\begin{aligned} \mathrm{F} &= \mathrm{A}, \\ \mathrm{G} &= (\mathrm{A_1} - \mathrm{A_2})\,\mathrm{X_q}, \\ \mathrm{H} &= \mathrm{C}, \\ \mathrm{E} &= (\mathrm{C_1} - \mathrm{C_2})\,\mathrm{X_q} \end{aligned} \tag{6}$$

where, X_q is the equilibrium state corresponding to the operating point. The equilibrium satisfies the averaged steady-state condition.

$$A\,X_q + B\,V_g = 0 \tag{7}$$

Solving for the equilibrium state yields:

$$X_q = -A^{-1}B\,V_g \tag{8}$$

To ensure accurate reference tracking with zero steady-state error, integral action is incorporated by augmenting the model with an additional state defined as the integral of the voltage tracking error:

$$\xi = \tilde{v}_{ref} - \tilde{v}_o \tag{9}$$

The augmented state vector is:

$$x_a(t) = \begin{bmatrix} \tilde{x}(t) \\ \xi(t) \end{bmatrix} \tag{10}$$

and the resulting augmented dynamics can be written as:

$$\dot{x}_a(t) = \hat{F}\,x_a(t) + \hat{G}\,\tilde{d}(t) + \begin{bmatrix} 0 \\ 0 \\ 1 \end{bmatrix} \tilde{v}_{ref} \tag{11}$$

with

$$\hat{F} = \begin{bmatrix} F & 0 \\ -H & 0 \end{bmatrix}, \qquad \hat{G} = \begin{bmatrix} G \\ -E \end{bmatrix} \tag{12}$$

This integral-augmented small-signal model is used in the subsequent section to synthesize the proposed controllers.

3. CONTROL DESIGN

This section presents the control framework adopted for output-voltage regulation of the Boost converter. The objective is to regulate the converter output around its nominal reference by manipulating the duty-ratio perturbation while preserving internal closed-loop stability under reference changes, input-voltage disturbances, and output-side loading perturbations. The proposed design is based on a mixed-sensitivity H_∞ controller synthesized from the nominal integral-augmented small-signal model, while an LQR controller designed from the same augmented model is used as a benchmark. To improve clarity, the H_∞ design is first introduced in its generalized-plant form, then verified in the frequency domain, and finally compared with the LQR benchmark.

3.1 Mixed-sensitivity H_∞ synthesis

The proposed H_∞ controller is synthesized from the nominal integral-augmented small-signal model derived in Section 2. Let $x_a = [\tilde{x}^T \quad \xi]^T$ denote the augmented state vector, where $\tilde{x}$ contains the converter state perturbations and ξ is the integral state associated with the output-voltage tracking error. For control synthesis, the nominal model is extended with the exogenous input vector:

$$w = [r \quad d_{vg} \quad d_{load}]^T \tag{13}$$

where, r is the reference input, d_{vg} is an input-voltage disturbance, and d_{load} is an equivalent load-disturbance input used to represent abrupt output-side load changes. The resulting synthesis model is written as:

$$\begin{aligned} \dot{x}_a &= \hat{F}\,x_a + \hat{G}\,u + B_w\,w, \\ y &= C_y\,x_a + D_{yu}\,u \end{aligned} \tag{14}$$

where, $u = \tilde{d}$ is the duty-ratio perturbation and y denotes the output-voltage perturbation.

The controller is formulated as a dynamic output-feedback law driven by the measured signal vector.

$$y_m = [\tilde{\imath}_L \quad y \quad \xi]^T, \qquad u = K(s)y_m \tag{15}$$

where, $\tilde{\imath}_L$ is the inductor-current perturbation. This structure allows the controller to exploit both current and voltage information while preserving the integral action required for zero steady-state tracking error.

To encode the design objectives in a unified frequency-domain framework, the tracking error is defined as:

$$e = r - y \tag{16}$$

and the weighted performance output is chosen as:

$$z = \begin{bmatrix} W_s e \\ W_u u \\ W_t y \end{bmatrix} \tag{17}$$

The mixed-sensitivity H_∞ problem then consists in determining a stabilizing controller K(s) that minimizes the closed-loop H_∞ norm from the exogenous input w to the regulated output z [12], namely

$$\min_{K(s)} \| T_{zw}(s) \|_\infty \tag{18}$$

The three weighting functions retain their standard interpretations. The weight W_s is used to improve low-frequency tracking accuracy and disturbance rejection, W_u penalizes excessive duty-ratio activity, and W_t enforces high-frequency roll-off of the regulated output in order to limit amplification of unmodeled fast dynamics. In this work, W_s and W_t are selected as low-order stable transfer functions, whereas W_u is chosen as a constant [11-13].

In the present study, the weighting functions are parameterized in the following first-order forms:

$$W_s(s) = \frac{s/M_s + \omega_b}{s + \omega_b A_s} \tag{19}$$

$$W_u(s) = 1/u_{max} \tag{20}$$

$$W_t(s) = \frac{s + \omega_t/M_t}{A_t s + \omega_t} \tag{21}$$

where, A_s and M_s determine the low-frequency sensitivity level and the allowable sensitivity peak, respectively, u_{max} specifies the admissible control activity, and A_t, M_t, and ω_T govern the complementary-sensitivity shaping at high

frequency. The frequency ω_b defines the desired sensitivity-shaping bandwidth [21-23].

Because the Boost converter is non-minimum phase, the weighting selection is carried out conservatively so that the implied closed-loop bandwidth remains compatible with the RHP zero of the duty-to-output dynamics. The resulting controller therefore provides a compromise among tracking performance, disturbance attenuation, and control moderation within a unified robust-control framework.

The frequency-domain behavior of the resulting H_∞ controller is examined next in order to verify that the achieved loop shaping is consistent with the intended regulation objectives and the non-minimum-phase limitation of the Boost converter.

3.2 Frequency-domain analysis of the mixed-sensitivity H_∞ design

The frequency-domain behavior of the proposed controller is now examined in order to verify that the achieved loop shaping is consistent with the intended regulation objectives and with the non-minimum-phase nature of the Boost converter. The following results correspond to the reults correspond to the final mixed-sensitivity H_∞ controller whose weighting parameters were optimized by the genetic-algorithm-based tuning procedure described later in Section 3.4.

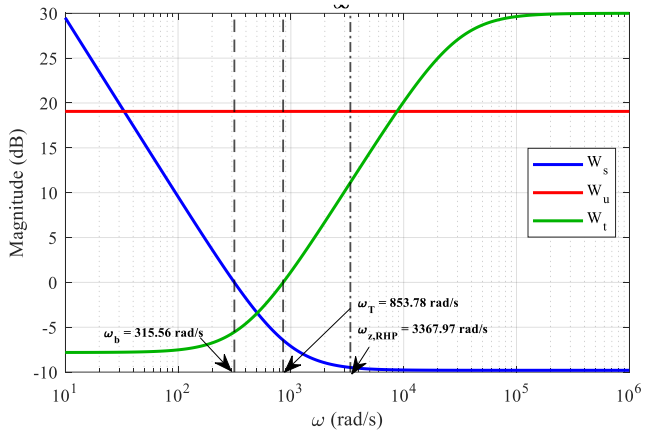

Figure 2. Mixed-sensitivity H_∞ weighting functions used for controller synthesis

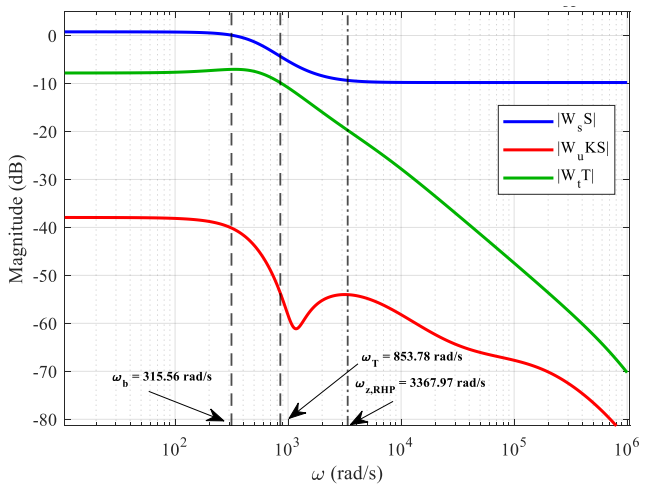

Figure 3. Frequency-domain verification of the mixed-sensitivity H_∞ design for the reference channel

Figure 2 shows the weighting functions used in the synthesis. The sensitivity weight W_s is shaped to enforce strong low-frequency regulation and disturbance attenuation, the constant weight W_u penalizes excessive duty-ratio activity, and the complementary-sensitivity weight W_t imposes high-frequency roll-off in order to reduce amplification of unmodeled fast dynamics. The corresponding shaping frequencies are $\omega_b = 315.56\ \mathrm{rad/s}$ and $\omega_T = 853.78\mathrm{rad/s}$, while the nominal RHP zero of the duty-to-output dynamics is located at $\omega_{z,\mathrm{RHP}} = 3367.97\ \mathrm{rad/s}$. Therefore, the effective shaping region remains well below the non-minimum-phase limitation of the Boost converter.

The achieved closed-loop behavior is verified in Figure 3 through the weighted maps W_sS, W_uKS, and W_tT, where S, KS, and T denote the sensitivity, control-sensitivity, and complementary-sensitivity functions, respectively. For the reference channel, the obtained norms are $\| W_sS \|_\infty = 1.092$, $\| W_uKS \|_\infty = 0.0127$, and $\| W_tT \|_\infty = 0.444$. These values confirm that the proposed controller achieves the intended frequency-domain compromise on the nominal plant: the sensitivity channel remains close to its desired low-frequency target, the control-effort channel is only weakly stressed, and the complementary-sensitivity channel is sufficiently attenuated at high frequency.

A channel-wise examination of the generalized closed-loop map provides additional insight into the achieved H_∞ shaping. The reference and input-voltage-disturbance channels exhibit moderate weighted amplification, whereas the equivalent load-disturbance channel remains the most demanding component of the generalized design. This observation is physically consistent with the nonlinear switched simulations reported later, in which abrupt load changes also constitute the most severe operating condition.

Overall, the frequency-domain analysis confirms that the proposed mixed-sensitivity H_∞ controller achieves the desired compromise among low-frequency voltage regulation, moderated control effort, and high-frequency attenuation, while respecting the bandwidth limitation imposed by the RHP zero of the Boost converter.

Having established the frequency-domain behavior of the proposed H_∞ controller, a benchmark design is introduced next in order to assess the extent to which the observed closed-loop improvement is attributable to the control methodology itself rather than to the underlying plant model.

3.3 Linear Quadratic Regulator benchmark

To provide a transparent baseline for comparison, an LQR controller is designed from the same nominal integral-augmented small-signal model used for the H_∞ synthesis. Specifically, the augmented dynamics defined in Eqs. (10)-(12) are used for the LQR design. The corresponding control law is expressed as [16, 22, 23]:

$$u = -\mathrm{K}_{\mathrm{LQR}}\mathrm{x}_a, \tag{22}$$

where, $\mathrm{K}_{\mathrm{LQR}}$ is the optimal state-feedback gain obtained by minimizing the quadratic cost function.

$$J = \int_0^\infty (\mathrm{x}_a^T \mathrm{Q} \mathrm{x}_a + u^T R u)\ dt. \tag{23}$$

The weighting matrix Q penalizes deviations of the augmented states, while R limits excessive control activity. In

particular, a relatively large weight is assigned to the integral state to enforce negligible steady-state tracking error, whereas the remaining state weights are selected to moderate transient overshoot and settling behavior. The scalar R is chosen to avoid overly aggressive duty-ratio variations.

Because the LQR benchmark is constructed from the same integral-augmented nominal model as the H_∞ controller, the subsequent comparison focuses on the effect of the control design methodology rather than on differences in plant representation. For both controllers, the physical duty ratio applied to the PWM stage is reconstructed from the nominal operating duty ratio and the control perturbation, with saturation enforced over the admissible interval.

3.4 Controller-parameter tuning by genetic algorithm

To avoid manual trial-and-error tuning and to ensure a fair comparison, the final parameters of both controller families were obtained using a common Genetic Algorithm (GA)-based outer-loop optimization procedure applied to the nominal integral-augmented small-signal model.

For each candidate parameter set, the corresponding controller was synthesized and evaluated under the same nominal closed-loop scenarios, namely reference tracking, input-voltage disturbance rejection, and equivalent load-disturbance rejection. The optimization objective was defined as the sum of the scenario-wise ITAE indices,

$$J_{GA} = \mathrm{ITAE}_{\mathrm{ref}} + \mathrm{ITAE}_{\mathrm{vg}} + \mathrm{ITAE}_{\mathrm{load}}, \qquad (24)$$

For the proposed controller, the GA tuned the parameters defining the weighting functions W_s, W_u, and W_t. For the benchmark controller, the GA tuned the diagonal entries of Q and the scalar R. The final retained parameters are summarized in Tables 1 and 2.

After fixing the final controller parameters through the common GA-based tuning procedure, both controllers were implemented in the nonlinear switched MATLAB/Simulink model for comparative validation under realistic operating conditions.

Table 1. Final Genetic Algorithm (GA)-tuned weighting parameters of the mixed-sensitivity H_∞ controller

Parameter	Description	Value
M_s	Sensitivity peak parameter	3.0903
A_s	Low-frequency sensitivity parameter	$10^{-5.2734}$
u_{max}	Admissible duty-ratio perturbation magnitude	0.1114
M_t	Complementary-sensitivity peak parameter	2.4583
A_t	High-frequency complementary-sensitivity parameter	$10^{-1.5}$
ω_b (rad/s)	Sensitivity-shaping frequency	315.56
ω_t (rad/s)	Complementary-sensitivity shaping frequency	853.78

Table 2. Final Genetic Algorithm (GA)-tuned Linear Quadratic Regulator (LQR) parameters

Quantity	Value
Q	$diag$ ([40.26 14.47 9.868×10^6])
R	2541
K_{LQR}	[0.2094 0.0772 -62.3178]

4. SIMULATION RESULTS AND ANALYSIS

This section validates the proposed mixed-sensitivity H_∞ controller in a nonlinear switched MATLAB/Simulink model of the Boost converter and compares its performance with the LQR benchmark. The objective is to assess reference-tracking performance, disturbance rejection, and implementation-oriented control behavior under the same operating conditions. To improve clarity, the simulation framework and performance indices are first defined, after which the results are discussed for reference changes, load disturbances, and input-voltage perturbations.

4.1 Simulation framework and performance criteria

The proposed mixed-sensitivity H_∞ controller and the LQR benchmark were evaluated in a nonlinear PWM switching model of the Boost converter operating in CCM. The regulated variable is the output voltage v_o, and the controller output is applied as a duty-ratio perturbation about the nominal operating point under saturation over the admissible duty interval. The converter parameters and nominal operating conditions used in the simulations are summarized in Table 3.

Table 3. Boost converter parameters and nominal operating conditions used in simulation

Parameter	Value
Input voltage (V_g)	56 V
Nominal output voltage (V_{ref})	200 V
Inductance (L)	602.11 µH
Capacitance (C)	27 µF
Load resistance (R_L)	26.66 Ω
Switching frequency (F_s)	50 kHz
Inductor resistance (r_L)	5 mΩ
Capacitor ESR (r_C)	50 mΩ
Switch on-resistance (r_{DS})	10 mΩ
Nominal equilibrium inductor current ($i_{L,eq}$)	27.067 A
Nominal equilibrium output voltage ($v_{o,eq}$)	199.939 V
Nominal duty ratio (D_{nom})	0.722924
Duty limits	$d \in$ [0.05 0.095]

Three test scenarios were considered.

- Scenario A evaluates reference tracking through a +10 step at t = 5 ms, followed by a -20 step at t = 50 ms.
- Scenario B evaluates load-disturbance rejection through a change from R_L to $R_L/2$ at t = 10 ms, followed by a change from $R_L/2$ to $2R_L$ at t = 60 ms.
- Scenario C evaluates input-voltage disturbance rejection through a -10 V input variation at t = 10 ms, followed by a +20 V variation at t = 60 ms.

These scenarios were selected to assess nominal tracking, output-side disturbance rejection, and line regulation under a unified switching-simulation framework. For consistency, the closed-loop responses were evaluated using transient, disturbance, integral-error, and actuator-related metrics, as summarized in Table 4.

Tracking indices are used for Scenario A, disturbance indices for Scenarios B and C, whereas integral, actuator, and ripple metrics are reported for all scenarios. The output-voltage responses are used as the primary performance figures, whereas the duty-ratio and inductor-current waveforms are used to interpret the associated control effort and internal current dynamics. The reference-tracking results are discussed

first, followed by the load- and line-disturbance cases, and finally by the actuator-related behavior.

Table 4. Closed-loop performance indices

Group	Indices
Tracking	t_r, M_p, t_s, SSE
Disturbance rejection	V_{min}, ΔV, t_{rec}, SSE
Integral error	IAE, ISE, ITAE
Actuator usage	RMS($d-D_{\text{nom}}$), $d_{\min}$, $d_{\max}$, time near saturation
Ripple	$\Delta v_{o,pp}$, $\Delta i_{L,pp}$

4.2 Reference-tracking performance

The reference-tracking performance is evaluated under Scenario A, the corresponding output-voltage, duty-ratio, and inductor-current responses are shown in Figure 4(a), Figure 5(a), and Figure 6(a), respectively, while the event-wise metrics are summarized in Table 5.

Both controllers achieve negligible steady-state tracking error, confirming the effectiveness of the integral augmentation. However, the mixed-sensitivity H_∞ controller yields a faster and better damped response in both step events. As reported in Table 5, its rise time remains close to 3.1 ms in both transitions, whereas the LQR benchmark requires about 6.8 to 7.0 ms. The overshoot is also markedly reduced, remaining below 0.5% for the proposed controller, while the LQR response reaches about 3.7% to 4.0%. The largest difference appears in the settling time, where the worst-case value is 6.7 ms for the mixed-sensitivity controller, compared with 44.88 ms for the LQR benchmark.

The same trend is reflected by the integral-error indices. Over the full reference-tracking profile, the mixed-sensitivity H_∞ controller gives lower IAE, ISE, and ITAE than the LQR benchmark, indicating that it reduces both instantaneous deviation and cumulative tracking error over the entire scenario. This confirms that the improvement is not limited to a single transient feature, but extends to the overall regulation quality.

From a control viewpoint, this behavior is consistent with the frequency-domain shaping established in Section 3. The mixed-sensitivity design explicitly constrains the low-frequency sensitivity while maintaining adequate high-frequency roll-off, which here translates into faster output correction and improved damping. By contrast, the LQR benchmark is intentionally more conservative, which reduces control aggressiveness but leads to slower tracking and larger transient excursions. This interpretation is also supported by the duty-ratio trajectories: the proposed controller uses a larger duty-ratio deviation than LQR, but both controllers remain well within the admissible interval and no time near saturation is observed in this scenario.

The inductor-current waveforms further clarify the transient mechanism. Under the mixed-sensitivity controller, the current is redistributed more rapidly after each reference change, which accelerates the energy transfer required to restore the output voltage. The LQR controller produces a smoother but slower current transition, which explains the longer settling behavior observed in the voltage response. Overall, under nominal reference changes, the mixed-sensitivity H_∞ controller provides the better compromise between speed, damping, and tracking accuracy, at the cost of increased but still admissible control activity.

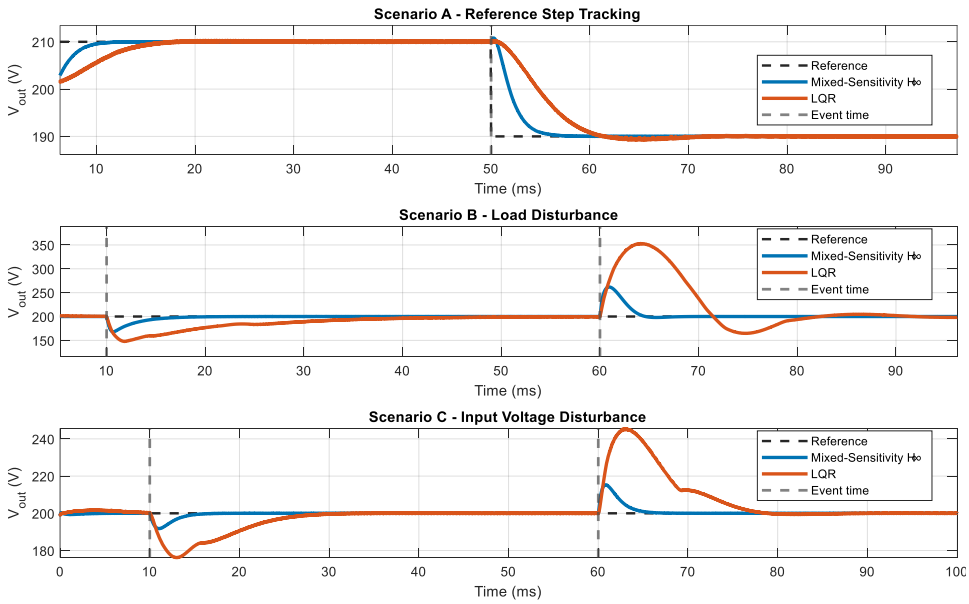

Figure 4. Output-voltage responses under (a) reference tracking, (b) load disturbance, and (c) input-voltage

Table 5. Reference-tracking metrics under Scenario A

Controller	Event	t_r (ms)	M_p (%)	t_s (ms)	SSE (V)	IAE	ISE	ITAE ($\times 10^{-4}$)
Mixed-Sensitivity H_∞	$V_{ref}+10V$	3.1718	0.4062	6.0174	0.0075	0.0227	0.1532	0.453
	$V_{ref}-20V$	3.0890	0.1346	6.0392	0.0121	0.0445	0.6068	0.791
Linear Quadratic Regulator (LQR)	$V_{ref}+10V$	7.0250	3.6680	44.875	0.0753	0.0496	0.2903	2.272
	$V_{ref}-20V$	6.8190	3.9820	19.375	0.0621	0.1070	1.4511	4.415

Table 6. Disturbance-rejection metrics under load and input-voltage disturbances

Controller	Event	$V_{\min}$ (V)	ΔV (V)	t_{rec} (ms)	SSE (V)	IAE	ISE	ITAE ($\times 10^{-4}$)
Mixed-Sensitivity H_∞	Load: $R_L \to R_L/2$	167.84	32.159	5.6896	0.0122	0.0942	1.7172	2.660
	Load: $R_L \to 2R_L$	197.99	2.0128	4.0230	0.0045	0.1491	6.6405	2.590
	Input: $V_g - 10$ V	191.76	8.2399	2.6296	0.0137	0.0221	0.1192	0.589
	Input: $V_g + 20$ V	199.97	0.0348	3.1946	0.0195	0.0371	0.3756	0.739
Linear Quadratic Regulator (LQR)	Load: $R_L \to R_L/2$	147.73	52.268	30.175	0.6326	0.6256	17.609	67.92
	Load: $R_L \to 2R_L$	164.70	35.299	27.875	0.5418	1.3517	139.88	97.56
	Input: $V_g - 10$ V	176.21	23.793	13.616	0.1409	0.1927	2.9243	12.66
	Input: $V_g + 20$ V	199.32	0.6839	14.997	0.0189	0.3464	10.570	20.21

4.3 Disturbance-rejection performance

The disturbance-rejection capability is evaluated under Scenario B and Scenario C, which correspond to abrupt load changes and input-voltage perturbations, respectively. The output-voltage responses are shown in Figure 4(b) and Figure 4(c), while the detailed event-wise metrics are reported in Table 6. The associated duty-ratio and inductor-current waveforms are discussed later in Section 4.5 from a practical implementation viewpoint.

Under load disturbances, the proposed mixed-sensitivity H_∞ controller preserves a substantially tighter voltage response than the LQR benchmark. For the most severe event, corresponding to $R_L \to R_L/2$ at t=10 ms, the minimum output voltage is limited to 167.84 V, with a voltage dip of 32.16 V and a recovery time of 5.69 ms. Under the same condition, the LQR controller drops to 147.73 V yielding a 52.27 V dip and a much longer recovery time of 30.18 ms. A similar transient behavior is observed for the second load event at t=60 ms, where the proposed controller reduces the voltage excursion to 2.01 V, whereas the LQR benchmark still exhibits a 35.30 V deviation and a recovery time of 27.88 ms. These differences are also reflected in the integral-error indices, for which the mixed-sensitivity H_∞ controller yields markedly lower IAE, ISE, and ITAE over the full load-disturbance scenario.

From a control viewpoint, this result is consistent with the generalized H_∞ design developed in Section 3. The equivalent load-disturbance channel was identified as the most demanding component of the nominal generalized plant, and this is precisely the operating condition in which the proposed controller provides the largest practical improvement. The faster recovery indicates that the controller restores the output-energy balance more rapidly after abrupt changes in output power demand, whereas the LQR benchmark remains stable but reacts more slowly, leading to deeper voltage dips and prolonged under-regulation.

A similar but less severe behavior is observed under input-voltage disturbances. For the -10 V input-voltage drop at t = 10 ms, the mixed-sensitivity H_∞ controller limits the minimum output voltage to 191.76 V, corresponding to an 8.24 V dip, while the LQR controller drops to 176.21 V, corresponding to a 23.79 V dip. The recovery time is also reduced from 13.62 ms to 2.63 ms. During the subsequent +20 V input variation at t=60 ms, both controllers maintain the output close to the nominal value, but the proposed controller again recovers faster and with lower accumulated error. The same conclusion is confirmed by the scenario-level integral metrics, which remain consistently lower for the mixed-sensitivity design than for the LQR benchmark.

Overall, the disturbance results show that the proposed controller improves both output-side and source-side regulation, with the largest performance gap appearing under abrupt load changes. This confirms that the mixed-sensitivity formulation is particularly effective in shaping the closed-loop response against the operating conditions that are most critical for the Boost converter.

4.4 Unified quantitative comparison

Tables 5-7 confirm that the mixed-sensitivity H_∞ controller outperforms the LQR benchmark in all tested scenarios. In reference tracking, it reduces the worst-case rise time from 7.0250 ms to 3.1718 ms, the worst-case overshoot from 3.9820 % to 0.4062 %, and the worst-case settling time from 44.8750 ms to 6.0392 ms. The scenario-level integral indices are also lower, indicating reduced cumulative tracking error.

The largest improvement appears under load disturbances. For the event $R_L \to R_L/2$, the proposed controller limits the voltage dip to 32.16 V and recovers in 5.6896 ms, whereas the LQR controller exhibits a 52.27 V dip and a 30.1750 ms recovery time. Under input-voltage disturbances, the same ordering is preserved: for the -10 V input-voltage drop, the mixed-sensitivity controller reduces the dip from 23.79 V to 8.24 V and the recovery time from 13.6160 ms to 2.6296 ms. These results are consistent with the generalized H_∞ design, for which disturbance attenuation, especially on the load side, is a dominant requirement.

These gains are achieved with higher, but still admissible, duty-ratio activity. The mixed-sensitivity controller yields larger RMS duty deviation in all scenarios, yet both controllers remain within the admissible duty interval and time near saturation is zero or negligible. Ripple levels also remain comparable, indicating that the faster regulation is not obtained at the expense of a significant ripple penalty. Overall, the unified metrics show that the proposed controller provides the best compromise among tracking speed, disturbance rejection, and practical actuator usage.

4.5 Practical control considerations

The duty-ratio and inductor-current responses provide an implementation-oriented interpretation of the preceding results. As shown by the actuator metrics in Table 7, the mixed-sensitivity H_∞ controller requires larger duty-ratio deviations than the LQR benchmark in all scenarios, with RMS $(\mathrm{d} - D_{\mathrm{nom}})$ ranging from 0.0638 to 0.0798, compared with 0.0130 to 0.0451 for LQR. This increase is expected, since the proposed controller is tuned to improve transient regulation and disturbance rejection. However, the control action remains practically admissible: the duty ratio stays within the imposed bounds in all cases, and time near saturation is either zero or negligible, reaching only 0.0234 ms (0.03%) in the most severe load-disturbance case.

The inductor-current waveforms clarify the mechanism

behind the improved voltage regulation. Under the mixed-sensitivity controller, the current is redistributed more rapidly after reference and disturbance events, which accelerates energy transfer to the output and shortens the voltage recovery interval. By contrast, the LQR benchmark produces smoother but slower current transients, consistent with its more conservative control action and longer settling or recovery times. Thus, the improved voltage performance of the proposed controller is directly associated with a faster internal current response.

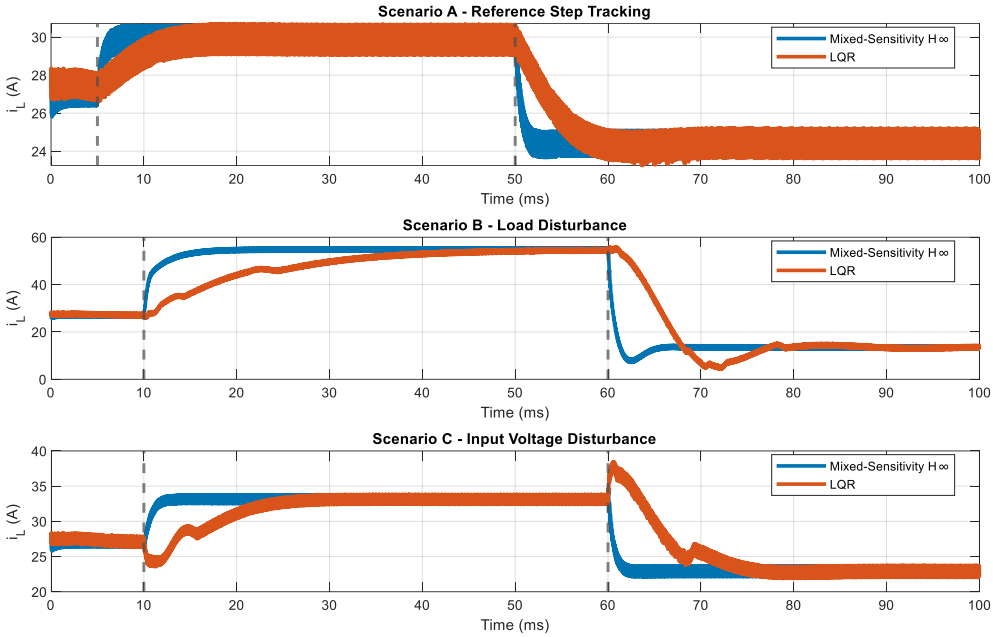

Figure 5. Inductor-current responses under (a) reference tracking, (b) load disturbance, and (c) input-voltage disturbance

Table 7. Actuator-usage and ripple metrics

Controller	Scenario	$RMS(d - D_{nom})$	d_{min}	d_{max}	Time Near Sat. (ms)	Time Near Sat. (%)	$\Delta v_{o,pp}$ (V)	$\Delta i_{L,pp}$ (A)
Mixed-Sensitivity H_∞	Step	0.0661	0.6169	0.8565	0	0	2.2059	1.3092
	Load	0.0638	0.5256	0.9422	0.0234	0.0234	1.1900	1.3445
	Input	0.0798	0.6169	0.8902	0	0	2.1220	1.4716
Linear Quadratic Regulator (LQR)	Step	0.0130	0.6942	0.7340	0	0	2.1957	1.3350
	Load	0.0432	0.5980	0.8524	0	0	1.2010	1.3803
	Input	0.0450	0.6460	0.7786	0	0	2.1037	1.4779

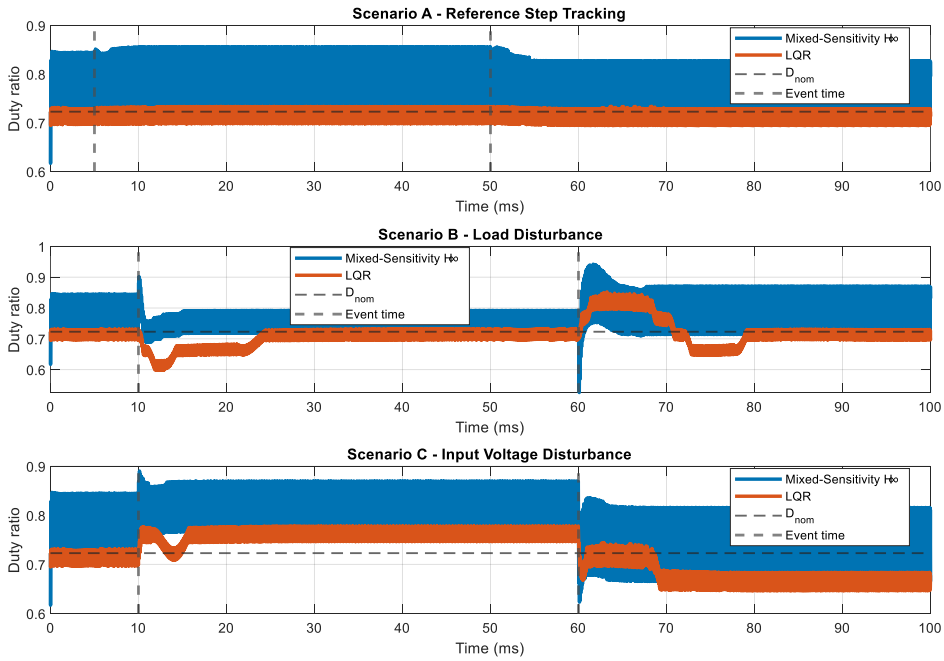

Figure 6. Duty-ratio responses under (a) reference tracking, (b) load disturbance, and (c) input-voltage

Despite the stronger duty-ratio activity, the ripple levels remain comparable between the two controllers. The output-voltage ripple stays close to 1.19-2.21 V, while the inductor-current ripple remains in the range 1.31-1.48 A for both designs. This indicates that the faster regulation achieved by the mixed-sensitivity controller is not obtained at the expense of a substantial switching-ripple penalty. Overall, the proposed controller improves dynamic performance while preserving acceptable actuator usage, saturation margin, and ripple behavior, which supports its practical applicability in Boost-converter voltage regulation.

5. CONCLUSION

This paper presented an integral-augmented mixed-sensitivity H_∞ controller for output-voltage regulation of a CCM Boost converter and evaluated it against an LQR benchmark derived from the same augmented nominal model. The study combined control-oriented modeling, frequency-domain verification, and nonlinear PWM switching simulations under reference variations, load disturbances, and input-voltage perturbations.

The comparative results show that the proposed controller provides the most favorable overall regulation behavior. Its main advantage is not only faster reference tracking, but also a clear reduction in disturbance-induced voltage excursions and recovery times, particularly under abrupt load changes. This behavior is consistent with the frequency-domain shaping of the sensitivity and complementary-sensitivity channels and with the identified importance of the equivalent load-disturbance channel in the generalized design.

At the same time, the improved dynamic performance is obtained with higher, but still admissible, duty-ratio activity. The controller remains within the imposed duty bounds, exhibits negligible time near saturation, and does not introduce a significant ripple penalty relative to the LQR benchmark. These results support the practical relevance of the proposed design for high-precision Boost-converter voltage regulation.

The present study is limited to simulation-based validation. Although the final assessment was carried out on a nonlinear PWM switching model rather than only on the nominal linear synthesis model, experimental verification is still required before drawing conclusions about hardware implementation. Future work will therefore focus on real-time experimental validation, extension to uncertainty-aware formulations over wider operating ranges, and investigation of digital implementation effects such as sampling, quantization, and PWM nonidealities.

REFERENCES

[1] Salehi, S.M., Varjani, A.Y. (2025). A new high voltage gain step-up converter with minimum phase characteristic. Scientific Reports, 15(1): 26842. https://doi.org/10.1038/s41598-025-12169-2

[2] Nadermohammadi, A., Abolhassani, P., Seifi, A., Zarrinehbafan, M., Aghakhanlou, P., Hosseini, S.H., Sabahi, M. (2024). Cost-effective soft-switching ultra-high step-up DC-DC converter with high power density for DC microgrid application. Scientific Reports, 14: 20407. https://doi.org/10.1038/s41598-024-71436-w

[3] Erickson, R.W., Maksimovic, D. (2001). Fundamentals of Power Electronics. 2nd ed. Kluwer Academic Publishers, Norwell, MA, USA.

[4] Emadi, A. (2004). Modeling and analysis of multiconverter DC power electronic systems using the generalized state-space averaging method. IEEE Transactions on Industrial Electronics, 51(3): 661-668. https://doi.org/10.1109/TIE.2004.825339

[5] Sanchis, R., Martín, J.M. (2026). PID tuning strategies for boost converters: Optimal compromise between performance and noise amplification. Mathematics and Computers in Simulation, 240: 381-402. https://doi.org/10.1016/j.matcom.2025.07.009

[6] Daoudi, L., Ourici, A., Ghoudelbourk, S. (2025). Control and energy management of hybrid renewable DC microgrid by using flatness method with predictive neural network and fuzzy PI regulation. Journal Européen des Systèmes Automatisés, 58(12): 2655-2663. https://doi.org/10.18280/jesa.581219

[7] Middlebrook, R.D., Ćuk, S. (1976). A general unified approach to modelling switching-converter power stages. In 1976 IEEE Power Electronics Specialists Conference, Cleveland, OH, USA, pp. 18-34. https://doi.org/10.1109/PESC.1976.7072895

[8] Leung, F.H.F., Tam, P.K.S., Li, C.K. (1991). The control of switching DC-DC converters—A general LWR problem. IEEE Transactions on Industrial Electronics, 38(1): 65-71. https://doi.org/10.1109/41.103487

[9] Skogestad, S., Postlethwaite, I. (2005). Multivariable Feedback Control: Analysis and Design. 2nd ed. John Wiley & Sons, Chichester, U.K.

[10] McFarlane, D., Glover, K. (1992). A loop-shaping design procedure using H∞ synthesis. IEEE Transactions on Automatic Control, 37(6): 759-769. https://doi.org/10.1109/9.256330

[11] Zhou, K., Doyle, J.C. (1998). Essentials of Robust Control. Prentice Hall, Upper Saddle River, NJ, USA.

[12] Gu, D.W., Petkov, P.H., Konstantinov, M.M. (2013). Robust Control Design with MATLAB®. 2nd ed. Springer, London, U.K. https://doi.org/10.1007/978-1-4471-4682-7

[13] Doyle, J.C., Francis, B.A., Tannenbaum, A.R. (1992). Feedback Control Theory. Macmillan Publishing Co., New York, NY, USA.

[14] Shaw, P., Veerachary, M. (2017). Mixed-sensitivity based robust H∞ controller design for high-gain boost converter. In Proceedings of the 2017 International Conference on Computer, Communications and Electronics (Comptelix), Jaipur, India, pp. 612-617. https://doi.org/10.1109/COMPTELIX.2017.8004042

[15] Keskin, R., Aliskan, I., Daş, E. (2021). Robust structured controller synthesis for interleaved boost converters using an H∞ control method. Transactions of the Institute of Measurement and Control, 43(14): 3169-3180. https://doi.org/10.1177/01423312211019560

[16] Alhosaini, W., Aldosari, O., Batiyah, S. (2025). Robust H-infinity control of a two-phase interleaved boost converter for second-life battery integration in battery energy storage systems. Frontiers in Energy Research, 13: 1689813. https://doi.org/10.3389/fenrg.2025.1689813

[17] Makhlouf, M., Laouar, O. (2025). Comparative analysis of bidirectional interleaved DC-DC boost converter control strategies. Journal Européen des Systèmes Automatisés, 58(9): 1911-1920. https://doi.org/10.18280/jesa.580913

[18] Hameed, H.Q., Hasan, F.A., Rashad, L.J. (2025). Robust H∞ control for master-slave power converters in renewable energy systems. e-Prime - Advances in Electrical Engineering, Electronics and Energy, 13: 101104. https://doi.org/10.1016/j.prime.2025.101104

[19] Ait Ramdane, N., Rahoui, A., Boukais, B., Benkhoris, M.F., Ait-Ahmed, M., Djerioui, A. (2024). Design and implementation of robust H∞ control for improving disturbance rejection of grid-connected three-phase PWM rectifiers. Energies, 17(9): 2166. https://doi.org/10.3390/en17092166

[20] Pal, B.C., Chaudhuri, B. (2005). Mixed-sensitivity approach using linear matrix inequalities. In Robust Control in Power Systems. Springer, Boston, pp. 115-138. https://doi.org/10.1007/0-387-25950-3_8

[21] Dupont, F., Montagner, V.F., Pinheiro, J.R., Péres, A. (2013). Comparison of linear quadratic controllers with stability analysis for DC-DC boost converters under large load range. Asian Journal of Control, 15(3): 861-871. https://doi.org/10.1002/asjc.561

[22] Bekkar, B., Ferkous, K. (2023). Design of online fuzzy tuning LQR controller applied to rotary single inverted pendulum: Experimental validation. Arabian Journal for Science and Engineering, 48(5): 6957-6972. https://doi.org/10.1007/s13369-022-06921-3

[23] Rantzer, A., Johansson, M. (2000). Piecewise linear quadratic optimal control. IEEE Transactions on Automatic Control, 45(4): 629-637. https://doi.org/10.1109/9.847100